Journal Name

ARTICLE TYPE

Cite this: DOI: 10.1039/xxxxxxxxxx

Dissimilar behavior of YAG:Ce and LuAG:Ce scintillator garnets regarding Li^+ co-doping

M.V. Derdzyan,[a] K.L. Hovhannesyan,[a] A.V. Yeganyan,[a] R.V. Sargsyan,[a] A. Novikov,[a] A.G. Petrosyan,[a*] and C. Dujardin [b*]

Received Date
Accepted Date

DOI: 10.1039/xxxxxxxxxx

www.rsc.org/journalname

Using a combination of experimental methods, the substitution tendencies of Li^+ and involved charge compensation mechanisms are determined and compared in two important similar scintillators, LuAG:Ce and YAG:Ce. The studies were performed on polycrystalline samples prepared by solid phase reactions as well as in single crystals grown by the vertical Bridgman method. The results show that Li^+ in LuAG:Ce,Li is localized mainly at Lu^{3+} sites with charge compensation brought about by $Ce^{3+} \rightarrow Ce^{4+}$ conversion and creation of anion vacancies. Surprisingly, unlike LuAG:Ce,Li, no evidence for Li^+ substitution at Y^{3+} sites and conversion of Ce^{3+} to Ce^{4+} has been obtained in YAG:Ce,Li. It suggests that Li^+ goes mainly to interstitial positions and does not interact with Ce^{3+}. From an application point of view, Li^+ co-doping of YAG:Ce is not efficient to improve the scintillation decay parameters, however, it is efficient to reduce the amount of anion vacancies in both YAG and YAG:Ce

1 Introduction

Because of the emerging and demanding needs in terms of ionizing radiation detection, the research on scintillating materials is continuously active regarding the impact of the crystal physical-chemical properties on the optical and scintillating mechanisms. In this context, co-doping of Ce-doped oxides with divalent impurities substituting for three-valence cation sites to favor Ce^{4+} states is among the most promising approaches developed in recent years to improve the time-response properties and the light yield of several types of scintillators important for medical imaging, homeland security and high-energy physics applications.[1] The scintillation mechanism involving Ce^{4+} has been considered in orthosilicates[2], several garnets[3–5] and yttrium perovskite[6]. The sequential charge capture of an electron hole pair by Ce^{3+} is generally described as: $Ce^{3+} + e^- + h^+ \rightarrow Ce^{4+} + e^- \rightarrow (Ce^{3+})^*$. Ce^{4+} is optically non-active under visible excitation (no 4f electron), but the sequential charge trapping scheme suggests that Ce^{4+} can also be seen as a preprepared cerium ready to trap a free electron. Ce^{4+} centers trap thus excited electrons directly from the conduction band leading to excited Ce^{3+} and their radiative recombination. Skipping the first hole trapping stage avoids the delays in hole trapping prior to electron trapping present in the case of Ce^{3+}. It results in acceleration of the decay and suppression of slow components. While Ce^{4+} is undesired for photoluminescence application, it becomes a good activator for scintillating applications. Emission arising from Ce^{4+}-doped crystal under ionizing radiation excitation and showing a similar spectral behavior as Ce^{3+}-doped crystal was earlier registered in cathodoluminescence of YAG:Ce,Ca in which all Ce ions were converted to the 4+ state[7]. The intense band appearing in absorption spectra at 250-260 nm upon divalent co-doping is considered as evidence of oxidation of a part of Ce^{3+} to Ce^{4+} and ascribed to charge transfer from the oxygen 2p orbitals of the valence band to the Ce^{4+} 4f orbitals.[2,3] Ce^{4+} is efficient to improve also the radiation hardness of some garnets[8–11], since this ion well competes in electron capture with other electron traps which, if activated, lead to damage of transmission in the range of emission. Co-doping of YAP:Ce perovskite with Ca^{2+} [6] also lowers the charge carrier trapping probability on defect sites and reduces the probability of delayed recombination processes in scintillation and also reduces significantly the rise time. However, contrary to garnets and orthosilicates in which Ca or Mg co-doping proved to be a useful way to improve the scintillation characteristics, in the case of YAP:Ce crystals the light yield is significantly decreased. Ca-induced partial oxidation of Ce^{3+} ions in this host leads to non-radiative energy transfer between Ce^{3+} and Ce^{4+}, reducing the luminescence efficiency. This approach therefore cannot be considered particularly useful for YAP:Ce. A positive charge deficiency in the lattice can be induced also by introduction of monovalent impurities. A few attempts have been so far made to evalu-

[a] *Institute for Physical Research, National Academy of Sciences, 0203 Ashtarak, Armenia. E-mail: pet@ipr.sci.am*
[b] *Université de Lyon, Université Claude Bernard Lyon 1, CNRS, Institut Lumière Matière, F-69622 Villeurbanne, France. E-mail:: christophe.dujardin@univ-lyon1.fr*
* corresponding authors

ate the efficiency of this approach regarding stabilization of Ce^{4+} states in different materials. Co-doping of Ce-doped garnets with Li^+ was recently reported in [12–14]. An increase of the absorption below 350 nm that could be related to formation of Ce^{4+} states has been recorded in LuAG:Ce,Li grown by micro-pulling [12] and in comparison to LuAG:Ce, the scintillation decay and the light yield of these crystals were improved. Acceleration of the decay was reported in LuAG:Ce,Li optical ceramics [13] and also attributed to partial conversion of Ce^{3+} to Ce^{4+}. The positive effect of co-doping with Li^+ on the decay acceleration and on the improvement of the timing resolution was demonstrated also in Cz-grown GAGG:Ce [14]. Finally, it should be mentioned that stable Ce^{4+} centers can be created also by air-annealing at high temperatures, as reported for YAG:Ce [15,16], LuAG:Ce, LuAG:Ce,Mg, YAP:Ce [16]. Summarizing the results, conversion of a part of Ce^{3+} ions to Ce^{4+} by either divalent or monovalent co-doping and/or air annealing is presently considered as one of the most efficient ways to improve the timing and scintillation yield performances of Ce-doped garnet scintillators. While cations with unit charge difference and nearly the same size, with respect to the three valence lattice cations they substitute, are easily tolerated in garnet hosts, the case of monovalent cations is less evident and little information is available on their substitution preferences in different garnets, charge compensation mechanisms and resulting functional role. In the present work the results of studies on YAG:Ce,Li garnet, in comparison to LuAG:Ce,Li, are presented. The tendencies of Li^+ localization within the lattice and charge balance maintenance in the two garnet hosts are discussed based on structural characteristics, optical properties, irradiation induced absorption, and scintillation timing characteristics. It is shown that YAG:Ce and LuAG:Ce garnets, similar in many respects, are expectingly not similar regarding monovalent co-doping with Li^+.

2 Experimental

Polycrystalline YAG:Ce,Li and LuAG:Ce,Li garnets were prepared by solid phase reactions (air, 1500 °C, 12 h). The concentration of impurities was varied in a wide range: Li (0 to 900 ppm), Ce (0 and 1 at. %); in total, around 20 compositions were prepared. High-purity (99.99 %) Y_2O_3, Lu_2O_3, CeO_2 and Al_2O_3 oxides were used in preparations. Li_2CO_3 (99.95 %) was added to the starting stoichiometric mixtures of $Y_{3-x}Ce_xAl_5O_{12}$ and $Lu_{3-x}Ce_xAl_5O_{12}$ (x=0 and 0.03). Single crystals of YAG:Ce,Li and LuAG:Ce,Li were grown by the vertical Bridgman method (or vertical directional crystallization) [17,18]. Crystallization processes were carried out at rates 1.0-1.3 mm/h under an enclosed Ar/H_2 atmosphere and using seed crystals oriented along the <100> axis. YAG:Ce,Ca crystals were also grown under similar conditions and used in comparative measurements. The unit cell lattice parameter (a_0) values of reacted powders were measured by X-ray diffraction (DRF-2.0 diffractometer; CuKα radiation) with a 0.001 Å accuracy. The diffraction spectra were analyzed for presence of extraneous phases. The quality of single crystals was inspected on optically polished plates using MPS-2 polarization microscope. Absorption spectra of crystals (d=2 mm) were measured with a Specord200+ spectrophotometer in the 200-800 nm range. Crystal plates (d=2 mm) are shown below in section 3.2. Selected samples were irradiated at 300 K up to 10 kGy dose (^{60}Co γ-ray ring shaped source with 1.25MeV photon energy and 504 Gy/h dose rate). Scintillation decay measurements were performed at 300 K under X-ray excitation using a picosecond pulsed laser (C10196; Hamamatsu Inc.) with 100 kHz and 0.2 mA, and YG11 interference filter. TCSPC module (PicoHarp 300) was adopted to analyze the temporal histogram for the counts.

3 Results and Discussion

3.1 Polycrystalline samples

The X-ray diffraction of polycrystalline samples (Ce=0; 1 at.%; Li=0 to 800 ppm) prepared by solid phase reactions confirm the formation of high quality garnet materials with only small amounts of extraneous phases; example data are shown on figure 1. For using the unit cell parameter (a_0) as a criterion of the substitution tendency, the results are shown on figure 2 and Table 1. The calculated unit cell parameters versus Li concentration for dodecahedral site (c-site) occupancy using the relationship [19] are also given on the graphs, as solid lines. The Shannon-Prewitt ionic radius of Li^+ in 8-fold coordination is 0.92 Å suggesting substitution at Y^{3+} (1.019 Å) sites in YAG, and at Lu^{3+} (0.977 Å) sites in LuAG [20]. The size difference between Li^+ (0.76 Å) and Al^{3+} (0.53 Å) in octahedral (a-site) coordination is much bigger. Examining the electronegativities (χ_i) [21,22], Li^+ (0.98) is closer to Y^{3+} (1.29) and Lu^{3+} (1.37), rather than to Al^{3+} (1.5).

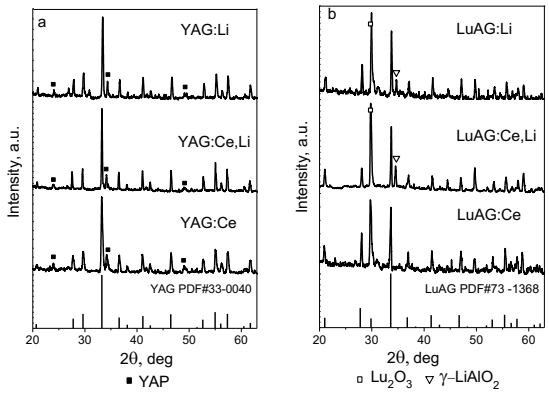

Fig. 1 X-ray diffraction of polycrystalline samples: (a) YAG:Ce,Li, (b) LuAG:Ce,Li

The change in unit cell parameter with Li concentration in LuAG:Li series (Fig.2-a) is very small giving no clear evidence for substitution by Li at any lattice site. There is evidence for c-site occupation by majority of Li^+ ions in LuAG:Ce,Li series; with addition of smaller Li^+ ion (relative to Lu^{3+}) the unit cell parameter decreases linearly from 11.913(7) Å(in LuAG:Ce) to 11.910(4) Å(in LuAG:Ce,Li 800 ppm) approximately obeying the Vegard's law [23] and the tilt angle between the calculated and measured dependences is only small. The positive charge deficiency compensation of Li^+ on a Lu^{3+} site is expected to be attained in

∗ calculated taking that all Ce are in the 4+ state

† calculated taking that all Ce are in the 4+ state and 1/3 of total Li^+ goes to a-sites

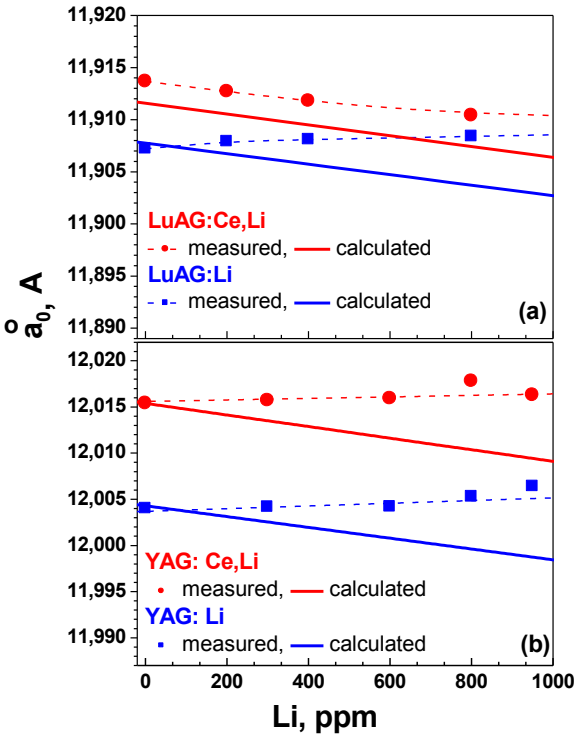

Fig. 2 Variation of unit cell parameter with Li concentration in reacted powders: (a) LuAG:Li and LuAG:Ce,Li, (b) YAG:Li and YAG:Ce,Li. Calculated dependences (solid lines) are derived using the relationship $a_0 = b_1 + b_2 r^{VIII} + b_3 r^{VI} + b_4 r^{IV} + b_5 r^{VIII} r^{VI} + b_6 r^{VIII} r^{IV}$.[19]

Table 1 Unit cell parameters and secondary phases in polycrystalline LuAG:Ce,Li and YAG:Ce,Li.

Ce %	Li ppm	secondary phase	a_0 Å(exp)	a_0 Å(calc)
LuAG:Ce,Li				
1	-	-	11.913(7)	11.9116
1	200	$LiAlO_2$ <0.1% $Lu2O_3$ traces	11.912(7)	11.9105
1	400	"	11.911(8)	11.9095
1	800	"	11.910(4)	11.9073
1	800	-	-	11.9034*
1	800	-	-	11.9104†
0	0	-	11.907(2)	11.9078
0	200	$LiAlO_2$ <0.2% $Lu2O_3$ traces	11.907(8)	11.9068
0	400	$LiAlO_2$ <0.5% $Lu2O_3$ traces	11.908(1)	11.9057
0	800	$LiAlO_2$ ~1% $Lu2O_3$ traces	11.908(4)	11.9039
YAG:Ce,Li				
1	-	$YAlO_3$ traces	12.015(4)	-
1	300	"	12.015(7)	-
1	600	"	12.015(9)	-
1	800	"	12.017(8)	-
1	950	"	12.016(3)	-
0	0	-	12.004	-
0	300	$YAlO_3$ traces	12.004(1)	-
0	600	"	12.004(2)	-
0	800	"	12.005(3)	-
0	950	"	12.006(4)	-

part by $Ce^{3+} \rightarrow Ce^{4+}$ conversion. Location of Li^+ at c-sites in presence of Ce indicates that the charge compensation of Li^+ on a Lu^{3+} site in LuAG:Ce,Li by $Ce^{3+} \rightarrow Ce^{4+}$ conversion is an energetically favorable option in this host gaining c-site substitution preference of Li^+. The unit cell parameter of the sample with 800 ppm of Li is slightly bigger than expected; some deviation from the calculated values indicates that at high concentrations a part of Li^+ ions may substitute for Al^{3+} at octahedral sites (Table 1). The difference between the calculated and measured unit cell parameters for LuAG:Ce (0.004 Å) is due to non-equivalent substitutions (not taken into account in calculations) showing that under applied experimental conditions around 1% of Lu is located at a-sites. The unit cell parameters in YAG:Li and YAG:Ce,Li series (Fig. 2-b) do not give evidence for substitution at any site of the lattice. In the case of c-site occupancy the unit cell parameter should decrease with Li concentration, while there is even a small increase which is however within or not far from the measurements error. It can be assumed that Li^+ ions in this host go to interstitial positions only slightly affecting the unit cell parameter.

Table 1 contains the measured unit cell parameters and identified secondary phases present in the samples. Non-similar substitution preferences of Li^+ in the two garnets studied here lead to different extraneous phases present in the samples. Only traces of secondary $YAlO_3$ phase are found in YAG:Li and YAG:Ce,Li evidencing that Li is absorbed by the lattice without violating the stoichiometry. Substitution at c-sites by majority of Li^+ ions in LuAG:Ce,Li series leads to an excess of c-cations and results in separation of Lu_2O_3 and $LiAlO_2$ phases. Higher secondary phase amounts in LuAG:Li, in comparison to YAG:Li, may be due to a lower solubility of Li in this host due to the smaller unit cell volume. Despite a number of approximations in the calculations of unit cell parameters plotted in Fig. 2 (the extent of non-equivalent substitutions and different valence states of Ce not taken into account), conclusions based on X-ray diffraction are further supported below by comparison of the color of YAG:Ce,Li and LuAG:Ce,Li samples.

The photographs of as-prepared example polycrystalline samples are given on figure 3. The greenish color of the LuAG:Ce,Li sample is clearly weaker than for the Li-free sample. It indicates that a part of Ce^{3+} ions (responsible for the green color) is converted to Ce^{4+} confirming the structural data (Fig.2-a) that the majority of Li^+ ions is located at Lu^{3+} sites. In contrast to this, there is no visible difference in the color between YAG:Ce and YAG:Ce,Li samples evidencing that no change in valence state of Ce^{3+} ions is observable; this fact indicates that Li^+ ions do not interact (or weakly interacts) with Ce^{3+} and therefore do not substitute for any lattice site. Prior work on optical properties of YAG:Nd,Li crystals has suggested that with Li incorporation the charge compensation is brought about by oxygen and that Li^+ ions are incorporated at interstitial positions without forming complexes with Nd[24]. Summarizing this section, the charge difference (2) between the host and co-dopant cations leads to non-similar substitution preferences and charge compensation mechanisms in the two studied garnets. Both the unit cell parameters and the color of polycrystalline samples indicate that, in contrast to LuAG:Ce,Li in which case the majority of Li^+ ions are located at lattice sites and favor $Ce^{3+} \rightarrow Ce^{4+}$ conversion, Li^+ ions in

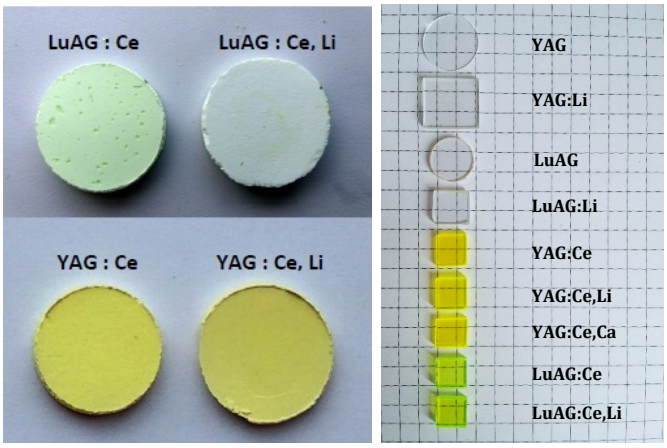

Fig. 3 Left: Photographs of polycrystalline LuAG:Ce(1 at%),Li(0; 400 ppm) and YAG:Ce(1 at%),Li(0; 400 ppm) samples prepared by solid phase reactions. Right: Photograph of variously doped LuAG and YAG samples.

YAG:Ce do not occupy any lattice site and do not interact with Ce, while the charge balance is maintained by reduction of anion vacancies.

3.2 Single crystals

Highly transparent single crystals of YAG:Ce,Li, LuAG:Ce,Li and YAG:Ce,Ca were obtained by the vertical Bridgman method. No additional visible defects have been found in YAG:Ce,Li(0-400 ppm), in comparison to those generally observed in YAG:Ce. The stress-birefringent patterns in longitudinal cuts of crystals revealing growth striations were similar to those usually seen in YAG:Ce. The grown LuAG:Ce,Li and YAG:Ce,Ca single crystals were also of high optical quality. The absorption spectra measured in different crystals are shown on figure 4. The main absorption bands at $\sim$ 200 nm, 340 nm and 457 nm are due to 4f-5d transitions of Ce^{3+}. All the spectra have been obtained from crystals cut from different boules to have similar content of Ce^{3+} (same absorption coefficient at 340 nm). This procedure enables to compare the induced UV absorption keeping the same amount of Ce^{3+} state. There is a distinct difference between YAG:Ce,Li and YAG:Ce in the UV range below 320 nm; the overall absorption in YAG:Ce,Li is lower (Fig 4-a). Conversion of a part of Ce^{3+} to Ce^{4+} should have led to an increase of absorption at 250-260nm, in comparison to that in YAG:Ce, as observed in the case of co-doping with divalent impurities (YAG:Ce,Ca, Fig. 4; YAG:Ce,Mg[25]. The optical absorption measurements do not therefore give any evidence for conversion of Ce^{3+} to Ce^{4+} and thus for any site occupation by Li^+. It should be mentioned that absorption in GGAG:Ce in the UV referred to Ce^{4+} is clearly enhanced by Li^+ co-doping[14]. Absorption below 350 nm in LuAG:Ce,Li grown by micro-pulling is also enhanced, more visible in the crystal with very high concentration of added Li[12]. In LuAG:Ce,Li optical ceramics[13], high absorption in the UV was attributed to various intrinsic defects and trace impurities, as well as to charge transfer absorption of Ce^{4+} created by Li^+ co-doping and air-annealing included in the preparation process. At low concentrations of Li^+, the absorption in the visible range of YAG:Ce and YAG:Ce,Li (Fig. 4-b) is nearly the same, but at high (400 ppm) Li concentrations an additional defect-related band appears in the range of Ce^{3+} emission which however can be removed by air-annealing. The wide band (Fig. 4-b, curve 3) may be associated with a kind of hole center, since it appears at very high concentrations of Li^+. It is consistent with the results reported for gamma irradiated YAG.[26] Comparison of YAG:Li with YAG-pure (Fig. 4-c) also shows a higher transparency in the UV in the Li containing sample.

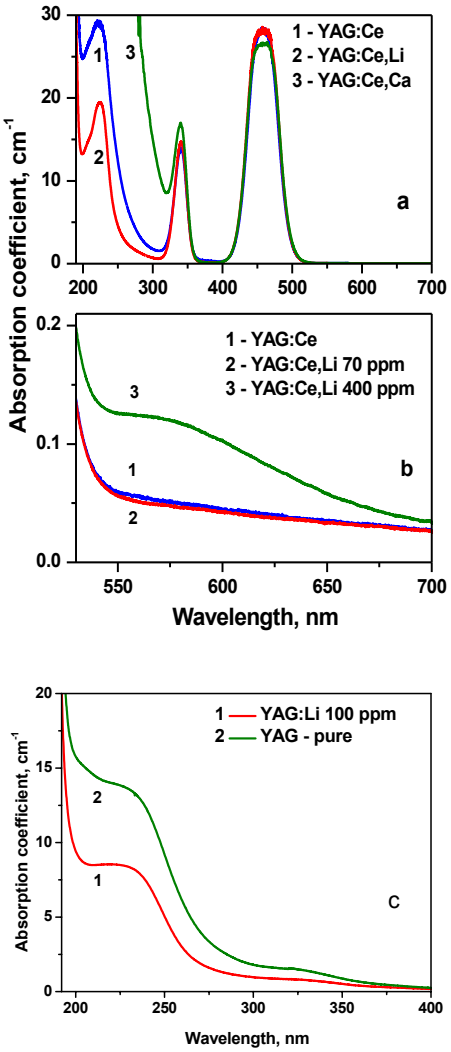

Fig. 4 (a) Absorption in YAG:Ce(0.15 at%), YAG:Ce(0.16 at%),Li(35 ppm) and YAG:Ce(0.13 at%),Ca(200 ppm); (b) absorption in YAG:Ce(0.3 at%), YAG:Ce(0.3 at%),Li(70 ppm) and YAG:Ce(0.3 at%),Li(400 ppm) in the visible range; (c) absorption in YAG-pure and YAG:Li(100 ppm) in the UV range.

Unlike YAG:Li (Fig. 4-c), introduction of Li to LuAG leads to an increase of absorption in the UV, evidencing that Li is incorporated at lattice sites increasing the amount of anion vacancies and associated defect centers (mainly F^+-type centers[27,28]) (Fig. 5-a). Higher absorption is seen also for LuAG:Ce,Li, in comparison to LuAG:Ce (Fig.5-b), in which Li favors $Ce^{3+} \rightarrow Ce^{4+}$ conversion

leading to an additional input to UV absorption, in agreement with[4,12]. The former fact (Fig. 5-a) shows that unlike the polycrystalline LuAG:Li, in which Li does not show clear evidence for occupation at any lattice site, in single crystals Li is incorporated at lattice sites increasing the number of defects associated with anion vacancies.

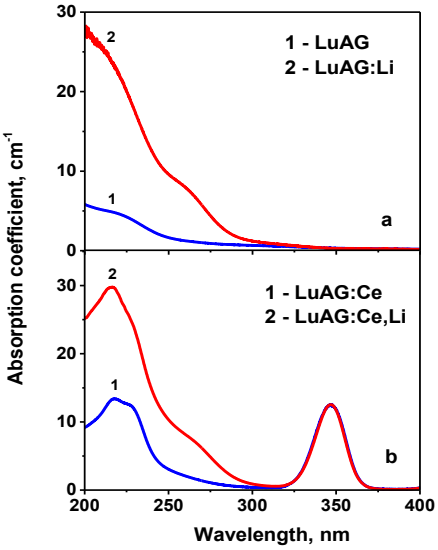

Fig. 5 Absorption in (a) LuAG and LuAG:Li(100 ppm), and (b) LuAG:Ce(0.09 at%) and LuAG:Ce(0.09 at%),Li(70 ppm).

Li co-doping leads to opposite effects in YAG:Ce and LuAG:Ce after γ-ray irradiation as well, Fig. 6(a,b). In YAG:Ce,Li induced absorption in the UV is lower, than in YAG:Ce. This fact also supports the conclusion that Li goes to interstitials reducing the amount of traps associated with anion vacancies. Despite the fact that a larger number of Ce^{3+} ions are converted to Ce^{4+} in Li co-doped samples in the course of irradiation (evidenced by a stronger decrease of absorption bands related to 4f-5d transitions of Ce^{3+}, Fig. 6-a), the absorption induced in the range at around 250 nm is lower, indicating that contribution of defects to absorption in this range is bigger than the contribution of Ce^{4+}. In LuAG:Ce,Li (Fig. 6-b) the induced absorption is higher, as compared to that in YAG:Ce,Li (Fig.6-a), supporting site occupation by Li^+ and higher weight of traps associated with anion vacancies. The opposite effects are also seen in YAG:Li and LuAG:Li, Fig. 6(c,d). Finally, Fig. 6-c (insert) also shows that Li doping of YAG decreases the induced absorption at 250-350 nm (maximum of the Cherenkov emission) by ~ 40 m^{-1}. A photograph of series of studied samples is given on Fig. 3. Summarizing this section, co-doping of LuAG:Ce with Li^+ leads to an increase of the optical absorption in the UV range below 350 nm giving evidence of formation of Ce^{4+} states resulting from substitution of Li^+ ions at Lu^{3+} sites and charge compensation maintained in part by $Ce^{3+} \rightarrow Ce^{4+}$ conversion. It should be mentioned that the positive charge deficiency in LuAG:Ce,Li may in addition lead

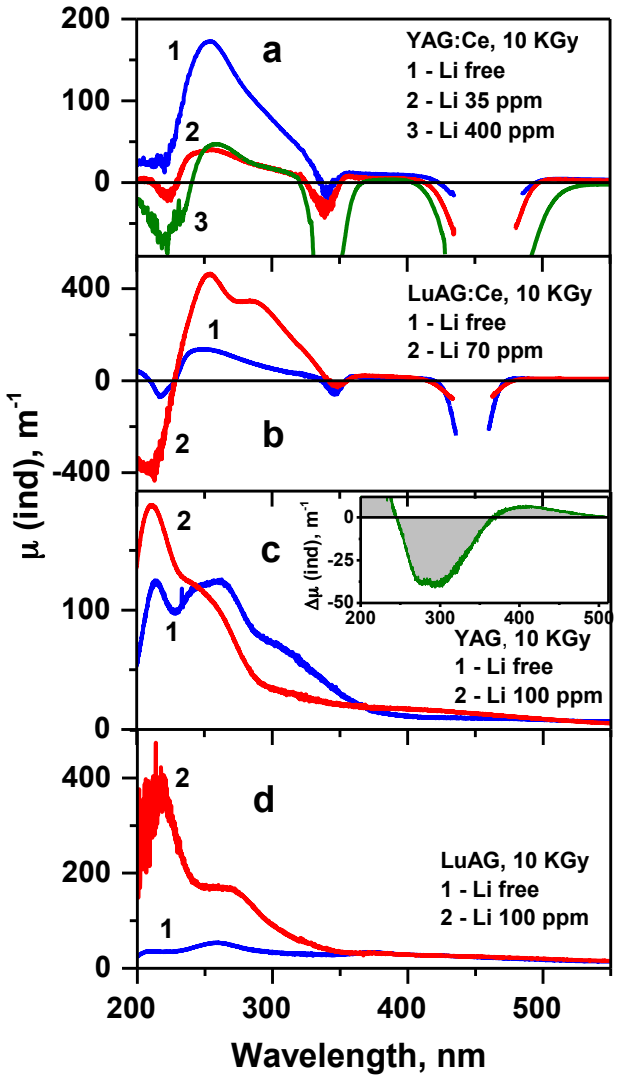

Fig. 6 γ-ray irradiation (10 kGy dose) induced absorption in: (a) YAG:Ce(0.2 at%), YAG:Ce(0.16 at%),Li(35 ppm), YAG:Ce(0.29 at%),Li(400 ppm); (b) LuAG:Ce(0.09 at%), LuAG:Ce(0.09 at%),Li(70 ppm); (c) YAG, YAG:Li(100 ppm); (d) LuAG, LuAG:Li(100 ppm).).

to creation of O^- centers, for charge balance, which were observed in ESR studies of LuAG:Ce,Mg[29]. Co-doping of YAG:Ce with Li^+ leads to decrease of absorption in the UV giving evidence that no change of the valence state of Ce^{3+} takes place, while the amount of traps associated with anion vacancies is decreased, both referred to preferable location of Li^+ at interstitials with charge compensation maintained by anion vacancies. Different effects of Li^+ co-doping take place also in the course of γ-ray irradiation of LuAG:Ce and YAG:Ce crystals supporting dissimilar incorporation and charge compensation mechanisms in these two garnets. The results correlate with measurements on polycrystalline samples discussed in section 3.1.

3.3 Scintillation decay

As demonstrated recently with YAP:Ce[6], the divalent Ca co-doping has significant impact on the time response under x-ray excitation. It acts on the decay time, the fraction of delayed emission and on the rise time. The probability of electron trapping is higher for Ce^{4+} than for Ce^{3+}, the balance between these two valence states modify thus the probability of trapping by defects. Because Ce^{4+} does not require hole trapping prior the emission of light, the balance between the 3+ and 4+ states of cerium changes the charge carrier migration distances responsible for the rise time. This effect is particularly evidenced at very low cerium content. In order to test the Li co-doping the scintillation decay has been measured under x-ray excitation for a set of YAG and LuAG sample for various cerium content and compared with Ca^{2+} co-doping and Li^{+} co-doping with respect to the slow component and to the rise time (Fig.7). In the case of YAG, in the range of concentration investigated, both the cerium concentration and the Li co-doping do not change significantly the rise time, which is only weakly decreased with Ca^{2+} co-doping. On the opposite, a slight shortening of the rise time is detected when the cerium content is increased from 0.065% to 0.28% and the Ca^{2+} co-doping clearly reduce the rise-time. When co-doped with Li^{+} and weakly doped with cerium, the measured rise time is similar to a non-co-doped LuAG but highly cerium doped, indicating an effect on the hole migration in the case of LuAG. The delayed luminescence under x-ray excitation reflects trapping effects. On the opposite to the rise time, the cerium content have a clear effect on the slow component amplitude in the case of YAG, while the cerium content has a very weak effect for LuAG. At equivalent cerium content, Li-codoping appears to slightly increase the amount of delayed luminescence for YAG while slightly decreases the for LuAG. On the opposite, Ca^{2+} co-doping clearly decreases the slow component amplitude in both cases. This dependence appears similar to that observed with Mg co-doping for $YAG:Ce^{3+}$.[25]

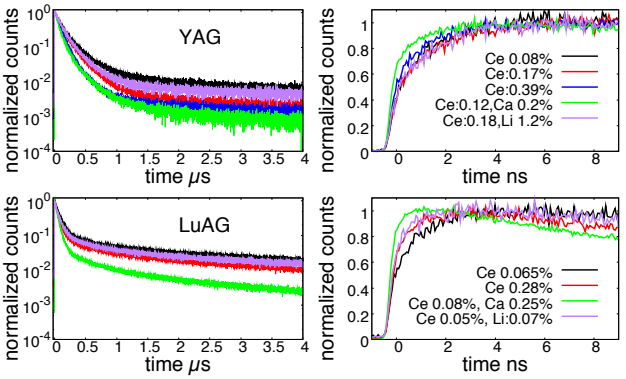

Fig. 7 X-ray induced luminescence decay time. Top figures correspond to YAG and bottom to LuAG. The left figures corresponds to large range over the first 4 μs, and the right figures to the first 8 ns to highlight the effect on the rise time.

4 Conclusions

YAG:Ce,Li and LuAG:Ce,Li have been prepared as polycrystalline samples by solid phase reactions and single crystals by the vertical Bridgman method. It is shown that Ce-doped LuAG and YAG garnets, similar in many respects, are not similar in respect to co-doping with Li. Basing on lattice parameters and the color of polycrystalline samples it is suggested that (a) Li^{+} ions in YAG:Ce,Li do not substitute for any lattice site and do not form complexes with Ce, but go to interstitials with charge compensation attained by reduction of anion vacancies, (b) Li^{+} ions in LuAG:Ce,Li do substitute for Lu^{3+} sites with charge balance attained in part by conversion of Ce^{3+} to Ce^{4+} and creation of O^{-} hole centers. The different incorporation preferences and charge compensation mechanisms of Li^{+} in these two garnet hosts have been further positively correlated with associated measurements on optical absorption and radiation induced absorption performed on single crystals. Among the probable explanations of differences between YAG and LuAG in respect to Li incorporation, we can mention the bigger unit cell volume of YAG and a bigger size difference between Y and Li ions. The results show that Li co-doping does not appear as an efficient way to improve the scintillation decay parameters of YAG:Ce, however it may be useful to reduce the number of anion vacancies in YAG and YAG:Ce and to increase the transparency and resistance to Îş-ray irradiation in the UV range. Co-doping of YAG:Ce at the same time with Ca^{2+} and Li^{+} may lead to both increase of desirable stable Ce^{4+} states and reduction of oxygen vacancies.

Acknowledgment

This work was performed in the scope of the International Associated Laboratory (CNRS-France & SCS-Armenia) IRMAS and of the European Union Horizon 2020 Programme under grant agreement no. 644260 (INTELUM).

References

1 M. Nikl and A. Yoshikawa, *Advanced Optical Materials*, 2015, **3**, 463–481.

2 S. Blahuta, A. Bessiere, B. Viana, P. Dorenbos and V. Ouspenski, *IEEE Transactions on Nuclear Science*, 2013, **60**, 3134–3141.

3 M. Nikl, K. Kamada, V. Babin, J. Pejchal, K. Pilarova, E. Mihokova, A. Beitlerova, K. Bartosiewicz, S. Kurosawa and A. Yoshikawa, *Crystal Growth & Design*, 2014, **14**, 4827–4833.

4 S. Liu, X. Feng, Z. Zhou, M. Nikl, Y. Shi and Y. Pan, *physica status solidi (RRL) - Rapid Research Letters*, 2014, **8**, 105–109.

5 Y. Wu, F. Meng, Q. Li, M. Koschan and C. L. Melcher, *Physical Review Applied*, 2014, **2**, 044009.

6 F. Moretti, K. Hovhannesyan, M. Derdzyan, G. A. Bizarri, E. D. Bourret, A. G. Petrosyan and C. Dujardin, *ChemPhysChem*, 2017, **18**, 493–499.

7 S. R. Rotman, H. L. Tuller and C. Warde, *Journal of Applied Physics*, 1992, **71**, 1209–1214.

8 M. Derdzyan, K. Ovanesyan, A. Petrosyan, A. Belsky, C. Dujardin, C. Pedrini, E. Auffray, P. Lecoq, M. Lucchini and K. Pauwels, *Journal of Crystal Growth*, 2012, **361**, 212–216.

9 A. Petrosyan, K. Ovanesyan, M. Derdzyan, I. Ghambaryan, G. Patton, F. Moretti, E. Auffray, P. Lecoq, M. Lucchini, K. Pauwels and C. Dujardin, *Journal of Crystal Growth*, 2015, **430**, 46–51.

10 Y. Shen, X. Feng, Y. Shi, A. Vedda, F. Moretti, C. Hu, S. Liu, Y. Pan, H. Kou and L. Wu, *Ceramics International*, 2014, **40**, 3715–3719.

11 S. Liu, X. Feng, Y. Shi, L. Wu, J. Luo, W. Wang and Y. Pan, *Optical Materials*, 2014, **36**, 1973–1977.

12 K. Kamada, M. Nikl, S. Kurosawa, A. Beitlerova, A. Nagura, Y. Shoji, J. Pejchal, Y. Ohashi, Y. Yokota and A. Yoshikawa, *Journal of Crystal Growth*, 2016, **452**, 85–88.

13 S. Liu, X. Feng, J. A. Mares, V. Babin, C. Hu, H. Kou, C. D'Ambrosio, J. Li, Y. Pan and M. Nikl, *Optical Materials*, 2017, **64**, 245–249.

14 K. Kamada, Y. Shoji, V. V. Kochurikhin, M. Yoshino, S. Okumura, S. Yamamoto, J. Y. Yeom, S. Kurosawa, Y. Yokota, Y. Ohashi, M. Nikl, M. Yoshino and A. Yoshikawa, *Optical Materials*, 2017, **65**, 52–55.

15 J. Bok, P. Horodyský and V. Krzyžánek, *Optical Materials*, 2015, **46**, 591–595.

16 M. Nikl, V. Babin, J. Mares, K. Kamada, S. Kurosawa, A. Yoshikawa, J. Tous, J. Houzvicka and K. Blazek, *Journal of Luminescence*, 2016, **169**, 539–543.

17 Chernov A. A., E. I. Givargizov, K. S. Bagdasarov, V. A. Kuznetsov, L. N. Demianets and A. N. Lobachev., *Crystal Research and Technology*, ger-verlag Berlin, Heidelberg, New York, Tokyo 1984, Sprin edn, 1985, vol. 20.

18 A. Petrosyan, *Journal of Crystal Growth*, 1994, **139**, 372–392.

19 B. Strocka, P. Holst and W. Tolksdorf, 1978, **33**, 186–202.

20 R. D. Shannon, *Acta Crystallographica Section A*, 1976, **32**, 751–767.

21 L. Pauling, *The Nature of the Chemical Bond*, Cornell University Press, 3rd edn, 1960.

22 K. Li and D. Xue, *The Journal of Physical Chemistry A*, 2006, **110**, 11332–11337.

23 L. Vegard, *Z. Phys.*, 1921, **5**, 17–26.

24 P. Arsenev, K. Binert, R. Francke, E. Kustov and I. Linda, *Phys. Stat. Sol. (a)*, 1973, **15**, year.

25 A. Nagura, K. Kamada, M. Nikl, S. Kurosawa, J. Pejchal, Y. Yokota, Y. Ohashi, Akira and Yoshikawa, *Japanese Journal of Applied Physics*, 2015, **54**, 04DH17.

26 M. Nikl, E. Mihokova, V. Laguta, J. Pejchal, S. Baccaro and A. Vedda, *Proceeding of SPIE*, 2007, 65860E.

27 M. Springis, A. Pujats and J. Valbis, *Journal of Physics: Condensed Matter*, 1991, **3**, 5457.

28 V. Babin, V. Laguta, A. Maaroos, A. Makhov, M. Nikl and S. Zazubovich, *physica status solidi (b)*, 2011, **248**, 239–242.

29 C. Hu, S. Liu, M. Fasoli, A. Vedda, M. Nikl, X. Feng and Y. Pan, *physica status solidi (RRL) - Rapid Research Letters*, 2015, **9**, 245–249.